Effect of interphase properties on the damping response of polymer nano-composites

ARTICLE *in* MECHANICS RESEARCH COMMUNICATIONS · JANUARY 2008

Impact Factor: 1.5 · DOI: 10.1016/j.mechrescom.2007.08.005

3 AUTHORS, INCLUDING:

Bishakh Bhattacharya
Indian Institute of Technology Kanpur
62 PUBLICATIONS **150** CITATIONS
SEE PROFILE

Sumit Basu
Indian Institute of Technology Kanpur
62 PUBLICATIONS **373** CITATIONS
SEE PROFILE

A Finite Element based investigation on obtaining high material damping over a large frequency range in viscoelastic composites

Rabindra Kumar Patel, Bishakh Bhattacharya and Sumit Basu [1]
Department of Mechanical Engineering, Indian Institute of Technology Kanpur,
Kanpur 208016, UP, India.

Abstract

Various vibration and noise suppression applications require a high loss factor ($\tan\delta$) over a wide frequency range. Homopolymers often do not meet this requirement. However, the damping properties of polymeric composites can be modulated to achieve this goal. In this paper we devise a simple Finite Element based unitcell model to calculate the effective $\tan\delta$ of a composite as a function of frequency. Using this method, we show that if the relaxation times of the constituents are properly chosen, a flat $\tan\delta$ response over a wide frequency range can be obtained.

Keywords: Composites; viscoelasticity; damping; loss factor; unitcell method

1 INTRODUCTION

Vibration and noise suppression applications include building structures under seismic excitation or wind loads [1], automobile, aerospace, house appliance industry, and railways [2] where mechanical vibrations of a wide frequency range are generated. To counteract the unwanted effect of vibration, broad-band vibration absorbers are required, which should have high damping capability over a wide frequency range [3]. For example, vibration of structures for general kind of loads, occur from about 0.1 Hz to 10 kHz depending on the size of the structure [4]. Ideal damping applications should provide a high loss factor $\tan\delta$ (either material or structural) over the entire range.

To achieve effective damping over a wide frequency range, various methods are used. Active [5] and semi-active vibration control techniques [6] magnetic vibration dampers [7] and particle dampers [8] can achieve high damping over wide range of frequencies. However, active damping usually suffers from spillover/waterbed effects. Magnetic and particle vibration dampers have larger weight penalty.

Passive damping using viscoelastic materials is simpler to implement and more cost-effective than semi-active and active techniques [9].

Passive damping techniques are extensively in use, in which viscoelastic (VE) polymers are used to reduce structure borne, airborne, and waterborne sound fields. Applications include free or constrained layer damping, both of which have been applied to a variety of situations, particularly in the aerospace industry. A US patent shows that a viscoelastic medium with fibers dispersed throughout eliminates the need for a constraining layer, thus reducing the size and weight of a damping treatment [10].

[1]Corresponding author Tel: +91 512 2597506; fax: +91 512 2597408; E-mail address: sbasu@iitk.ac.in

As is well known, homopolymers exhibit a high material damping response over a relatively narrow range of temperature and frequency. Methods used for achieving a wide $\tan\delta$ vs. frequency response include the use of copolymers, blending with other polymers [11], or inorganic materials [12] and even grafting. A more recent development is the interpenetrating polymer network (IPN) which is a novel class of polymer alloys where two or more crosslinked polymers are held together by physical entanglements [13]. A particularly interesting member of this group of materials is the gradient IPN, where a broad $\tan\delta$ over a temperature range of 273 - 373 K has been reported [14]. It should be noted that a gradient polymer can be treated as a polymer composite with a large number of viscoelastic phases.

In order to estimate the effective $\tan\delta$ of a polymeric composite, homogenization techniques have been extensively used. Hashin [15] has given bounds for macroscopic moduli of two or multiphase elastic heterogeneous materials. Later he extended the analysis to predict the macroscopic behaviour of heterogeneous linear viscoelastic media [16]. Christensen [17] has also derived analytical expressions for upper and lower bounds of the effective complex shear modulus of a linear viscoelastic matrix containing spherical voids or perfectly rigid spherical inclusions. Better estimates of the macroscopic viscoelastic properties can be obtained by using the Mori-Tanaka model [18] or other mean-field homogenization schemes [19]. Unitcell techniques used within the framework of the Finite Element (FE) method [18,19] offers an alternate route towards determining the effective loss and storage moduli as well as $\tan\delta$ of viscoelastic composites.

The first objective of this work is to develop a simple computational technique for determining effective $\tan\delta$ of a polymeric composite material (given its morphology) from unitcell analysis. Additionally, using the devised technique we show that by carefully selecting the viscoelastic properties of the constituents, the $\tan\delta$ vs. frequency response of the composite can be suitably modulated. This aids in realizing the aim of obtaining a high $\tan\delta$ value over a wide range of frequencies.

The present paper is organised in the following way. Section 2.1 and 2.2 explains the computational procedure adopted for solving a viscoelastic initial-boundary value problem using FE techniques. In Sec. 2.3 we outline the simple procedure adopted for extracting $\tan\delta$ of the composite from a unitcell analysis. Salient results obtained using this technique on a simple morphology are presented in Secs. 3.1 and 3.2.

2 COMPUTATIONAL PROCEDURE

In this work an initial/boundary value problem (IVBP) has been solved, for evaluating the effective damping behaviour of viscoelastic heterogeneous materials. Variables of state which are used to assess the response of material are displacement $\boldsymbol{u}(\boldsymbol{x},t)$, the stress tensor $\boldsymbol{\sigma}(\boldsymbol{x},t)$ and strain tensor $\boldsymbol{\epsilon}(\boldsymbol{x},t)$. In absence of body forces the governing equation which has to be solved is,

$$\boldsymbol{\nabla}\cdot\boldsymbol{\sigma}=\boldsymbol{0}. \tag{1}$$

Assuming small strains the strain displacement relations are,

$$\boldsymbol{\epsilon}=\frac{1}{2}(\boldsymbol{\nabla}\cdot\boldsymbol{u}+\boldsymbol{\nabla}\cdot\boldsymbol{u}^{T}), \tag{2}$$

and the constitutive equation for viscoelastic medium reads,

$$\boldsymbol{\sigma} = \int_{t_0}^{t} \boldsymbol{C}(\boldsymbol{x}, t - t') \frac{\partial \boldsymbol{\epsilon}(\boldsymbol{x}, t')}{\partial t'} dt', \tag{3}$$

where $\boldsymbol{C}(\boldsymbol{x}, t)$ is the viscoelastic constitutive tensor, t_0 initial time, t time of observation, and t' is the variable of integration.

Constraints imposed on the solution by boundary and initial conditions are,

$$\boldsymbol{u} = \boldsymbol{u}_0 \text{ on } \Gamma_u, \tag{4}$$

$$\boldsymbol{T} = \boldsymbol{\sigma}^T \boldsymbol{n} = \boldsymbol{T}_0 \text{ on } \Gamma_t,\ \Gamma_u \cup \Gamma_t = 0, \tag{5}$$

where $\boldsymbol{T_0}$ is the applied traction on Γ_t. On the remaining part of the boundary (i.e. Γ_u) displacement $\boldsymbol{u_0}$ is specified, and $\boldsymbol{n}$ is unit normal to the boundary, as shown in Fig. 1. For $t < t_0$,

$$\boldsymbol{u}(\boldsymbol{x}, t) = \boldsymbol{0} \text{ and, } \boldsymbol{\sigma}(\boldsymbol{x}, t) = \boldsymbol{0}. \tag{6}$$

2.1 Incremental Form of the Constitutive Equation

In order to avoid solving a set of Volterra integrals for the FE solution, numerical incrementalisation of the constitutive equation developed by Zocher *et al.* [20] has been used in this formulation. Use of this numerically approximated constitutive equation leads to a simple set of algebraic equations. Steps involved in deriving the incremental constitutive equation are outlined here for the sake of completeness.

The time line is subdivided into discrete intervals such that $t_{n+1} = t_n + \Delta t$. At the n^{th} and $(n+1)^{th}$ time steps the constitutive relations are given by,

$$\boldsymbol{\sigma}(\boldsymbol{x}, t_n) = \int_0^{t_n} \boldsymbol{C}\left(\boldsymbol{x}, t_n - t'\right) \frac{\partial \boldsymbol{\epsilon}\left(\boldsymbol{x}, t'\right)}{\partial t'} dt', \tag{7}$$

and,

$$\boldsymbol{\sigma}(\boldsymbol{x}, t_{n+1}) = \int_0^{t_{n+1}} \boldsymbol{C}\left(\boldsymbol{x}, t_{n+1} - t'\right) \frac{\partial \boldsymbol{\epsilon}\left(\boldsymbol{x}, t'\right)}{\partial t'} dt', \tag{8}$$

respectively.
Eq. (8) can also be written as,

$$\begin{aligned} \boldsymbol{\sigma}(\boldsymbol{x}, t_{n+1}) \;=\; & \int_0^{t_n} \boldsymbol{C}\left(\boldsymbol{x}, t_{n+1} - t'\right) \frac{\partial \boldsymbol{\epsilon}\left(\boldsymbol{x}, t'\right)}{\partial t'} dt' \\ & + \int_{t_n}^{t_{n+1}} \boldsymbol{C}\left(\boldsymbol{x}, t_{n+1} - t'\right) \frac{\partial \boldsymbol{\epsilon}\left(\boldsymbol{x}, t'\right)}{\partial t'} dt'. \end{aligned} \tag{9}$$

Thus, defining $\Delta\boldsymbol{\sigma}$ as,

$$\Delta\boldsymbol{\sigma} = \boldsymbol{\sigma}(\boldsymbol{x}, t_{n+1}) - \boldsymbol{\sigma}(\boldsymbol{x}, t_n), \tag{10}$$

and $\Delta\boldsymbol{C}$ as,

$$\Delta\boldsymbol{C} = \boldsymbol{C}\left(\boldsymbol{x}, t_{n+1} - t'\right) - \boldsymbol{C}\left(\boldsymbol{x}, t_n - t'\right), \tag{11}$$

where $\boldsymbol{C}$ is fitted with Wiechert model in the form,

$$\boldsymbol{C}(\boldsymbol{x}, t - t') = \boldsymbol{C}_\infty + \sum_{r=1}^{N} \boldsymbol{C}_r \exp\left(-(t - t')/\rho_r\right), \tag{12}$$

where the quantity N in represents number of spring-dashpot combinations in the model. Substituting Eqs. (7 and 9) in Eq. (10), it can be expressed as,

$$\begin{aligned} \Delta\boldsymbol{\sigma} &= \int_0^{t_n} \left(\boldsymbol{C}\left(\boldsymbol{x}, t_{n+1} - t'\right) - \boldsymbol{C}\left(\boldsymbol{x}, t_n - t'\right)\right) \frac{\partial \boldsymbol{\epsilon}\left(\boldsymbol{x}, t'\right)}{\partial t'} dt' \\ &\quad + \int_{t_n}^{t_{n+1}} \boldsymbol{C}\left(\boldsymbol{x}, t_{n+1} - t'\right) \frac{\partial \boldsymbol{\epsilon}\left(\boldsymbol{x}, t'\right)}{\partial t'} dt'. \end{aligned} \tag{13}$$

Therefore,

$$\Delta\boldsymbol{\sigma} = \int_{t_n}^{t_{n+1}} \boldsymbol{C}\left(\boldsymbol{x}, t_{n+1} - t'\right) \frac{\partial \boldsymbol{\epsilon}\left(\boldsymbol{x}, t'\right)}{\partial t'} dt' + \Delta\boldsymbol{\sigma}^{\boldsymbol{R}}, \text{ where} \tag{14}$$

$$\Delta\boldsymbol{\sigma}^{\boldsymbol{R}} = \int_0^{t_n} \Delta\boldsymbol{C} \frac{\partial \boldsymbol{\epsilon}\left(\boldsymbol{x}, t'\right)}{\partial t'} dt'. \tag{15}$$

For the plane strain case, in which we are particularly interested,

$$\boldsymbol{C}_\infty = \frac{E_\infty}{(1+\nu)(1-2\nu)} \begin{pmatrix} (1-\nu) & \nu & 0 \\ \nu & (1-\nu) & 0 \\ 0 & 0 & (1-2\nu) \end{pmatrix}, \tag{16}$$

and,

$$\boldsymbol{C}_r = \frac{E_r}{(1+\nu)(1-2\nu)} \begin{pmatrix} (1-\nu) & \nu & 0 \\ \nu & (1-\nu) & 0 \\ 0 & 0 & (1-2\nu) \end{pmatrix}, \tag{17}$$

where E_∞ is the long term relaxation modulus, and ν, the Poisson's ratio is assumed to be time independent. In addition, $\rho_r = \eta_r / E_r$, where η_r are dashpot coefficients and E_r are spring stiffnesses of the r^{th} spring-dashpot combination in the Wiechert model. The ρ_r are referred to as relaxation times.

Equation (14) can be further integrated in closed form to produce:

$$\Delta\boldsymbol{\sigma} = \boldsymbol{C}'\Delta\boldsymbol{\epsilon} + \Delta\boldsymbol{\sigma}^{R}, \tag{18}$$

where,

$$\boldsymbol{C}' = \boldsymbol{C}_\infty + \frac{1}{\Delta t} \sum_{r=1}^{N} \rho_r \boldsymbol{C}_r \left(1 - \exp(-\Delta t/\rho_r)\right), \tag{19}$$

and,

$$\Delta\boldsymbol{\sigma}^{R} = -\sum_{r=1}^{N} \left(1 - \exp\left(-\Delta t/\rho_r\right)\right) \int_0^{t_n} \exp\left(-(t_{n+1} - t')/\rho_r\right) \boldsymbol{C}_r \frac{\partial \boldsymbol{\epsilon}\left(\boldsymbol{x}, t'\right)}{\partial t'} dt'. \tag{20}$$

Equations (18-20) form the corner stone of the incremental FE formulation. Note that $\boldsymbol{C}'$ is a constant (as in a linear elastic analysis) if the time step Δt is fixed.
For the time interval $(t_n - \Delta t \leq t' \leq t_n)$ the strain rate $\boldsymbol{R}$ is approximated as,

$$\frac{\partial \boldsymbol{\epsilon}\left(\boldsymbol{x}, t'\right)}{\partial t'} \simeq \frac{\Delta \boldsymbol{\epsilon}}{\Delta t} \simeq \boldsymbol{R}.$$

Now Eq. (20) can be simplified as,

$$\boldsymbol{\Delta\sigma}^R = -\sum_{r=1}^{N} \left(1 - \exp(-\Delta t/\rho_r)\right) \boldsymbol{S}_r(\boldsymbol{x}, t_n), \tag{21}$$

where again for plane strain conditions,

$$\boldsymbol{S}_r(\boldsymbol{x}, t_n) = \int_0^{t_n} \exp(-\left(t_{n+1} - t'\right)/\rho_r) \tag{22}$$

$$\times \frac{E_r}{(1+\nu)(1-2\nu)} \begin{pmatrix} (1-\nu) & \nu & 0 \\ \nu & (1-\nu) & 0 \\ 0 & 0 & (1-2\nu) \end{pmatrix} \boldsymbol{R} dt'. \tag{23}$$

In addition, the $\boldsymbol{S}_r(\boldsymbol{x}, t_n)$ satisfies the recursive relation,

$$\boldsymbol{S}_r(\boldsymbol{x}, t_n) = \exp(-\Delta t/\rho_r) \boldsymbol{S}_r(\boldsymbol{x}, t_{n-1})$$

$$+ \left(1 - \exp(-\Delta t/\rho_r)\right) \frac{E_r \rho_r}{(1+\nu)(1-2\nu)} \begin{pmatrix} (1-\nu) & \nu & 0 \\ \nu & (1-\nu) & 0 \\ 0 & 0 & (1-2\nu) \end{pmatrix} \boldsymbol{R}. \tag{24}$$

2.2 Finite Element Formulation

In absence of body forces, virtual work rate equation for small deformation can be written as,

$$\int_V \delta \dot{\boldsymbol{\epsilon}}^T \boldsymbol{\sigma} dV = \int_S \delta \boldsymbol{v}^T \boldsymbol{T} dS. \tag{25}$$

Usual finite element assumptions are made as:

$$\boldsymbol{v}(\boldsymbol{x}, t) = \boldsymbol{N}\dot{\boldsymbol{U}}, \text{ and} \tag{26}$$

$$\dot{\boldsymbol{\epsilon}}(\boldsymbol{x}, t) = \boldsymbol{B}\dot{\boldsymbol{U}}, \tag{27}$$

within each element, where $\boldsymbol{U}$ is the vector of nodal displacements, $\boldsymbol{N}$ is the shape function matrix and $\boldsymbol{B}$ is the strain - displacement matrix.
Standard FE procedures for small strain leads to the incremental equation,

$$\int_V \boldsymbol{B}^T \Delta\boldsymbol{\sigma} dV = \int_S \boldsymbol{N}^T \Delta\boldsymbol{T} dS. \tag{28}$$

With the use of equation (18), eq. (28) becomes,

$$\int_V \boldsymbol{B}^T (\boldsymbol{C}' \Delta\boldsymbol{\epsilon} + \Delta\boldsymbol{\sigma}^R) dV = \int_S \boldsymbol{N}^T \Delta\boldsymbol{T} dS. \tag{29}$$

which, in turn, can be written as,

$$\int_V \boldsymbol{B}^T \boldsymbol{C}' \boldsymbol{B} \Delta \boldsymbol{U} \, dV + \int_V \boldsymbol{B}^T \Delta \boldsymbol{\sigma}^R dV = \int_S \boldsymbol{N}^T \Delta \boldsymbol{T} dS, \tag{30}$$

or,

$$\boldsymbol{K} \Delta \boldsymbol{U} = \Delta \boldsymbol{F} - \Delta \boldsymbol{\chi}, \tag{31}$$

where $\boldsymbol{K} = \int_V \boldsymbol{B}^T \boldsymbol{C}' \boldsymbol{B} dV$, is the global stiffness matrix. The first term on the right hand side of Eq. (31) is the vector containing the external load increments, and $\Delta \boldsymbol{\chi}$ is the time dependent contribution due to viscoelasticity.

2.3 Unitcell Technique

One of the objectives of this work is to determine the effective damping factor $\tan \delta^c$ of a microstructured material. To this end a unitcell technique is employed. The unitcell, which in principle may represent any microstructure, is subjected to special boundary conditions that ensure that "straight edges remain straight". The Rayleigh - Ritz technique is used to implement these boundary conditions as outlined in [21].

Though the above formulation does not restrict the morphology of the composite, in this preliminary analysis we adopt a square arrangement of cylindrical inclusions. With cross-section as shown in Fig. 2(a). In view of the reflective and translational symmetries, the shaded unitcell can be simplified to the one shown in Fig. 2(b). Note that symmetry boundary conditions are imposed on the edges $x_1 = 0$ and $x_2 = 0$. Results presented in the next section all pertain to this particular morphology. The unitcell is subjected to (see Fig. 2(b)) uniform normal macrostresses,

$$\Sigma_1(t) = \frac{1}{H} \int_0^H \sigma_{11}(t) dx_2 \text{ and } \Sigma_2(t) = \frac{1}{B} \int_0^B \sigma_{22}(t) dx_1, \tag{32}$$

where $\sigma_{ij}(t)$ are microstresses. The $\tan \delta^c$ can be obtained in the following way. Consider a macrostress state $\Sigma_2(t) = 0$ and $\Sigma_1(t) = \Sigma_0 \sin \omega t$. Then for a viscoelastic material, the macrostrain response $\bar{\epsilon}_1$ is given by

$$\bar{\epsilon}_1 = \frac{1}{BH} \int_V \epsilon_{11}(t) dV, \tag{33}$$

lags the macrostress by a time $\Delta\tau$ as shown in Fig. 2(c). Thus, as $t \to \infty$ the effective damping factor becomes,

$$\tan \delta^c \simeq \tan(\omega \Delta \tau). \tag{34}$$

This equation becomes exact for $t \gg$largest relaxation time.

3 RESULTS AND DISCUSSION

In this section we analyse composites with viscoelastic matrices and elastic or viscoelastic inclusions using the FE technique outlined above. The objective of the results presented

hereafter is to provide a 'proof of concept' of the fact that the damping response of a composite can be 'designed' appropriately by a suitable choice of viscoelastic material properties of the constituents.

In particular, we demonstrate that, by adding suitable inclusions in a matrix, it is possible in principle to modify its damping response to be high over a wide frequency range. To this end, the simple microstructure described in Sec. 2.3 will be used.

Since our purpose is to provide a 'proof of concept', we use the standard linear solid (SLS) with a one term Prony series representation, $E(t) = E_\infty + E_1 e^{-t/\rho_1}$ (see Eq. (12)).

In this work, the superscript 'm' is used to denote matrix quantities and 'c' for effective quantities pertaining to the composite. Superscript 'p_1', 'p_2' etc are used for the reinforcing phases. Thus, Prony series representations of the moduli of the matrix, first phase and second phase of the composite are $E^m(t) = E^m_\infty + E^m_1 e^{-t/\rho^m_1}$, $E^{p_1}(t) = E^{p_1}_\infty + E^{p_1}_1 e^{-t/\rho^{p_1}_1}$, and $E^{p_2}(t) = E^{p_2}_\infty + E^{p_2}_1 e^{-t/\rho^{p_2}_1}$ whereas that for $\tan\delta$ are $\tan\delta^m$, $\tan\delta^{p_1}$ and $\tan\delta^{p_2}$ respectively. For the composite, the effective $\tan\delta$ is denoted by $\tan\delta^c$.

3.1 Effective Damping Response of Composites

For a standard linear solid having modulus of the form $E(t) = E_\infty + E_1 e^{-t/\rho_1}$, a simple calculation shows that the maximum attainable $\tan\delta$ is $0.5(R^2+R)^{-1/2}$, which is achieved at a frequency of $\sqrt{(R)}/(2\pi\rho_1\sqrt{(1+R)})$ Hz, where $R = E_\infty/E_1$. The bandwidth of $\tan\delta$ response can be defined as the frequency range within which $\tan\delta$ is 70% of its maximum value. For a typical homopolymer like high impact polystyrene, for example, the bandwidth turns out to be only about 0.0023 Hz [22].

The approximate response of this SLS, when reinforced with inclusions can be obtained by applying the correspondence principle to the Voigt or Reuss estimates for the effective moduli. More sophisticated homogenization schemes are also available [18,19]. Thus, applying the correspondence principle to the Voigt estimate, for a 2-phase composite, the $\tan\delta^c$ is given by:

$$\tan\delta^c = \left(v^{p_1}\tan\delta^{p_1} + v^m \frac{E'^m}{E'^{p_1}}\tan\delta^m\right) \Big/ \left(v^{p_1} + \frac{E'^m}{E'^{p_1}} v^m\right) \tag{35}$$

where v^{p_1}, v^m and E'^{p_1}, E'^m volume fractions and storage moduli of inclusion and matrix respectively. For SLS, E'^{p_1} and E'^m can be expressed as

$$E'^{p_1} = E^{p_1}_\infty + E^{p_1}_1 \frac{\omega^2(\rho^{p_1}_1)^2}{1+\omega^2(\rho^{p_1}_1)^2},$$

and,

$$E'^m = E^m_\infty + E^m_1 \frac{\omega^2(\rho^m_1)^2}{1+\omega^2(\rho^m_1)^2},$$

respectively. Using the above estimate, the $\tan\delta^c$ response is plotted for a particular pair of viscoelastic materials in Fig. 3, where it is clear that the peaks of the $\tan\delta^c$ vs. ω response now occurs at two values of ω instead of one.

However, if the added inclusions are elastic (i.e. $E^{p_1}_1 = 0$), always $\tan\delta^c \le \tan\delta^m$. This is demonstrated in Fig. 4 on the basis of the Voigt estimate. We define a quantity α as,

$$\alpha = \frac{\max(\tan\delta^c)}{\max(\tan\delta^m)}. \tag{36}$$

In Fig. 4, the variation of α has been plotted against v^{p_1}. The maximum damping achievable in the composite for $E_\infty^{p_1} \neq 0$ is always lower than that of the matrix. In fact, with increase in v^{p_1} and $E_\infty^{p_1}$, α drops significantly below unity. Also as $E_1^{p_1} = 0$, Eq. (35) shows only one peak instead of two.

To achieve $\alpha > 1$ we need to use viscoelastic inclusions i.e. $E_1^{p_1} \neq 0$. This is demonstrated in Fig. 5 where again α has been plotted against $E_1^m/E_1^{p_1}$ for a viscoelastic-viscoelastic composite. Clearly, according to the Voigt estimate, for $E_1^m/E_1^{p_1} \lesssim 1.5$, $\alpha > 1$ is achievable. Thus Figs. 4 and 5 demonstrate that achieving high damping capacity and stiffness are somewhat contradictory objectives. While elastic inclusions help us to achieve the latter, they are rather ineffective as damping enhancers [23].

3.2 Modulation of the $\tan\delta$ vs. ω Response of Composites

We now turn to the results of actual FEM unitcell calculations where a square arrangement of cylindrical inclusions has been used. Figure 6 shows the $\tan\delta - \omega$ response of the matrix with $E^m(t) = 1 + 2e^{-t/0.1}$ MPa and Poisson's ratio $\nu^m = 0.33$. Expectedly, $\tan\delta^m$ peaks at a frequency of $\omega = 0.9$ Hz and $\max(\tan\delta^m) = 0.5773$.

Addition of elastic inclusions with $E_\infty^{p_1} = 100$ MPa and $\nu^{p_1} = 0.33$, again expectedly causes $\max(\tan\delta^c)$ to drop. On the other hand if 30% of the composite is voided (continuous curve in Fig. 6), there is almost no modification of the $\max(\tan\delta^c)$ value over $\max(\tan\delta^m)$. These results are in keeping with the predictions presented on the basis of the simple Voigt estimates.

The product of the stiffness $|E^c| = |E'^c + iE''^c|$ and $\tan\delta^c$ has been plotted in Fig. 7. Lakes [23] considers this quantity to be a proper figure of merit for damping materials. Figure 7 shows that $|E^c|\tan\delta^c$ is much higher for the composite with elastic inclusions, compared to the matrix. This figure underlines the beneficial effect of using elastic inclusions as a means of achieving a judicious compromise between stiffness and damping properties. However, elastic inclusions are not considered further in this paper as they are ineffective in flattening the $\tan\delta^c$ response.

Shape of the inclusions however, has a significant effect on $\tan\delta^c$. The effect of variation in $\tan\delta^c$ with shape is obviously not captured by the simple Voigt model (see Figs. 3-5). A somewhat better idea about the effect of shape is afforded by Fig. 8, where $\tan\delta^c$ is presented as a function of v^{p_1} for different shapes of inclusions. The results are obtained from unitcell simulations using the four morphologies shown in the inset. Cross-sections of inclusions which are more elongated along the direction of loading (i.e. x_1) give the highest $\tan\delta^c$. On the other hand, cross-sections of the inclusions that are elongated in a direction perpendicular to the load yield the least $\tan\delta^c$ values. Thus for elliptical inclusions (d) shows a much lower $\tan\delta^c$ than (c).

From the discussion above, it is clear that elastic inclusions (or voids) are not very beneficial in modifying the damping of the composite. Shape and morphology control, (to an extent more sophisticated than what is attempted here) may lead to somewhat improved $\tan\delta^c$. However, widening of the $\tan\delta^c$ - ω response is not possible by controlling only the shape or the elastic properties of the inclusions. This view is supported both by detailed FEM calculations as well as by simple Voigt estimates of $\tan\delta^c$.

The principle of flattening the $\tan\delta^c - \omega$ response is simple and is demonstrated here.

Figure 9 shows the responses of the matrix and composites. The matrix properties are $E^m(t) = 1 + 2e^{-t/0.1}$ MPa (same as in Fig. 6) while the inclusions have $E^{p_1}(t) = 1 + 30e^{-t/0.0005}$ MPa. Note that in the example chosen, $\rho_1^m/\rho_1^{p_1} = 200$. Simple calculation shows that the frequency corresponding to the $\tan\delta$ peak for the matrix occurs at $\omega^m = 0.9$ Hz and for inclusion at $\omega^{p_1} = 57$ Hz. The $\tan\delta^c - \omega$ response of the composite with $v^{p_1} = 0.3$ exhibits two distinct peaks at $\omega_1^c = 1$ Hz and $\omega_2^c = 40$ Hz. This is due to the fact that ρ^m and ρ^{p_1} are spaced such that $|1/\rho^m - 1/\rho^{p_1}| \gg$ bandwidth of either the matrix or the inclusion. If this condition is not satisfied, two distinct peaks do not result.

The flattening of the response in Fig. 9 can be achieved by adding sufficient volume fraction of a third phase with a relaxation time ρ^{p_2} such that,

$$\rho^{p_1} \leq \rho^{p_2} \leq \rho^m. \tag{37}$$

To demonstrate this, we have used a coating of a third material on the inclusion. The coating has properties $E^{p_2}(t) = 1 + 20e^{-t/0.005}$ MPa and $v^{p_2} = 0.25$ where ρ^{p_2} is in accordance with Eq. (37). The coating may represent the interphase region that exists between inclusion and matrix in polymeric composites [18]. Addition of the coating leads to a flatter response of $\tan\delta^c$ shown in Fig. 9. Thus, by using a 3-phase viscoelastic composite, a reasonably flat $\tan\delta^c$ response is obtained over the 1-100 Hz frequency range with a sacrifice in peak value in the range of 5%. The flatness is achieved primarily by spacing the relaxation times of the constituents appropriately. Further the volume fractions and thus morphology also need to be adjusted.

In principle, flatness of $\tan\delta^c$ over a larger frequency range can also be achieved by this technique. This can be done by simply using multiphase materials (e.g. a graded IPN) with a wide range of relaxation times. In Fig. 10 we show the results obtained for a fictitious composite material that has inclusions with graded relaxation times. Here we demonstrate the first attempts at morphology control to achieve a flat $\tan\delta^c$ response over a large frequency range. In this figure three additional phases have been used. These phases are arranged in concentric circles around phase p_1. All these four phases have almost similar moduli but their relaxation times range from $10^{-5}-10^{-2}$ s. The matrix properties remain the same as in Figs. 6 and 9. The response obtained for this multiphase composite is reasonably high over the range $1 - 10^4$ Hz. The flatness of the curve over this entire range however cannot be ensured without optimising the volume fractions v^{p_n} and moduli $E_1^{p_n}$ of the phases. We are currently working on a systematic procedure for performing this optimization.

4 CONCLUSION

In this work a unitcell based FE procedure for determining the effective $\tan\delta^c$ response of multiphase composite materials is proposed.

The procedure is applied to the determination of $\tan\delta^c$ for simple morphologies of polymeric composites with standard linear solid constituents. In the process it is demonstrated that by judiciously choosing the viscoelastic constituents and their morphology, a flat $\tan\delta^c$ versus ω response can be obtained over a wide frequency range.

The more involved 'inverse problem' of designing a morphology given the $\tan\delta^c$ vs. ω response and the material properties of the constituents, will be the subject of a future paper.

REFERENCES

1. Ye, K., Li, L., and Tang, J. (2003). Stochastic Seismic Response of Structures with Added Viscoelastic Dampers Modeled by Fractional Derivative, *Earthquake Engineering and Engineering Vibration*, **2**(1):133-139.

2. Castellani, A. (2000). Vibrations Generated by Rail Vehicles: A Mathematical Model in the Frequency Domain, *Vehicle System Dynamics*, **34**(3):153-173.

3. Yamada, N., Shoji, S., Sasaki, H., Nagatani, A., Yamaguchi K., Kohjiya, S., and Hashim, A.S. (1999). Developments of High Performance Vibration Absorber from Poly(vinyl chloride)/Chlorinated Polyethylene/Epoxydized Natural Rubber Blend, *Journal of Applied Polymer Science*, **71**(6):855-863.

4. Lakes, R.S. (1998). *Viscoelastic solids*, CRC Press, Boca Raton, Florida.

5. Jang, J.L., and Tarng, Y.S. (1999). A Study of the Active Vibration Control of a Cutting Tool, *Journal of Materials Processing Technology*, **95**(1-3):78-82.

6. Taniwangsa, W. and Kelly, J.M. (1997). Experimental Testing of a Semi-Active Control Scheme for Vibration Suppression, *Proceedings of the SPIE - The International Society for Optical Engineering*, **3045**:130-9.

7. Hansaka, M. and Mifune, N. (1994). Development of a New Type High Grade Damper: Magnetic-Vibration-Damper, *Quarterly Report of Railway Technical Research Institute (Japan)*, **35**(3):199-201.

8. Liu, W., Tomlinson, G. and Worden, K. (2002). Nonlinearity Study of Particle Dampers, *Proceedings of the 2002 international Conference on Noise and Vibration Engineering, ISMA*, Sep 16-18, Leuven, Belgium, Publisher :Katholieke Universiteit Leuven :495-499.

9. Rao, M.D. (2003). Recent Applications of Viscoelastic Damping for Noise Control in Automobiles and Commercial Airplanes, *Journal of Sound and Vibration*, **262**:457-474.

10. Thomas, E.A. and Yung, C. (1993). US patent: Fiber Enhancement of Viscoelastic Damping Polymers, Patent Number: 5,256,223.

11. Guang-Su, H., Lu-Xia, J. and Qiang, L. (2002). Molecular Design of Damping Rubber Based on Polyacrylate-Containing Silicone, *Journal of Applied Polymer Science*, **85**:746-751.

12. Vassileva, E. and Friedrich, K., (2003). Epoxy/Alumina Nanoparticle Composites: Dynamic Mechanical Behaviour. *Journal of Applied Polymer Science*, **89**:3774-3785.

13. Qin, Chuan-Li, Cai, Wei-Min, Cai, J., Tang, Dong-Yan, Zhang, Ju-Sheng, and Qin, M. (2004). Damping Properties and Morphology of Polyurethane/Vinyl Ester Resin Interpenetrating Polymer Network, *Materials Chemistry and Physics*, **85**:402-409.

14. Lipatov, Y.S., Karabanova, L.V. (1995). Gradient Interpenetrating Polymer Networks, *Journal of Materials Science*, **30**(10):2475-2484.

15. Hashin, Z. (1962). The Elastic Moduli of Heterogeneous Materials, *Journal of Applied Mechanics*, **29**:143-150.

16. Hashin, Z. (1965). Viscoelastic Behaviour of Heterogeneous Media, *Journal of Applied Mechanics-Transactions of the ASME 32E*, :630-663.

17. Christensen R.M. (1969). Viscoelastic Properties of Heterogeneous Media, *Journal of the Mechanics and Physics of Solids*, **17**:17-41.

18. Fisher, F.T., and Brinson, L.C. (2001). Viscoelastic Interphases in Polymer-Matrix Composites: Theoretical Models and Finite-Element Analysis, *Composites Science and Technology*, **61**:731-748.

19. Friebel, C., Doghri, I., and Legat, V. (2006). General Mean-Field Homogenization Schemes for Viscoelastic Composites Containing Multiple Phases of Coated Inclusions, *International Journal of Solids and Structures*, **43**:2513-2541.

20. Zocher, M.A. and Groves, S.E. (1997). A Three-Dimensional Finite Element Formulation for Thermoviscoelastic Orthotropic Media, *International Journal for Numerical Methods in Engineering*, **40**:2267-2288.

21. Van der Burg, M.W.D., and Van der Giessen, E. (1994). Delaunay-Network Modelling of Creep Failure in Regular Ploycrystalline Aggregates by Grain Boundary Cavitation, *International Journal of Damage Mechanics*, **3**:111-139.

22. Hummel, S.C. Hossain, K. and Hayes, G.T. (2001). Biaxial Stress Relaxation of High Impact Polystyrene Above the Glass Transition Temperature, *Polymer Engineering and Science*, **41**(3):566-574.

23. Lakes, R.S. (2002). High Damping Composite Materials: Effect of Structural Hierarchy, *Journal of Composite Materials*, **36**(3):287-297.

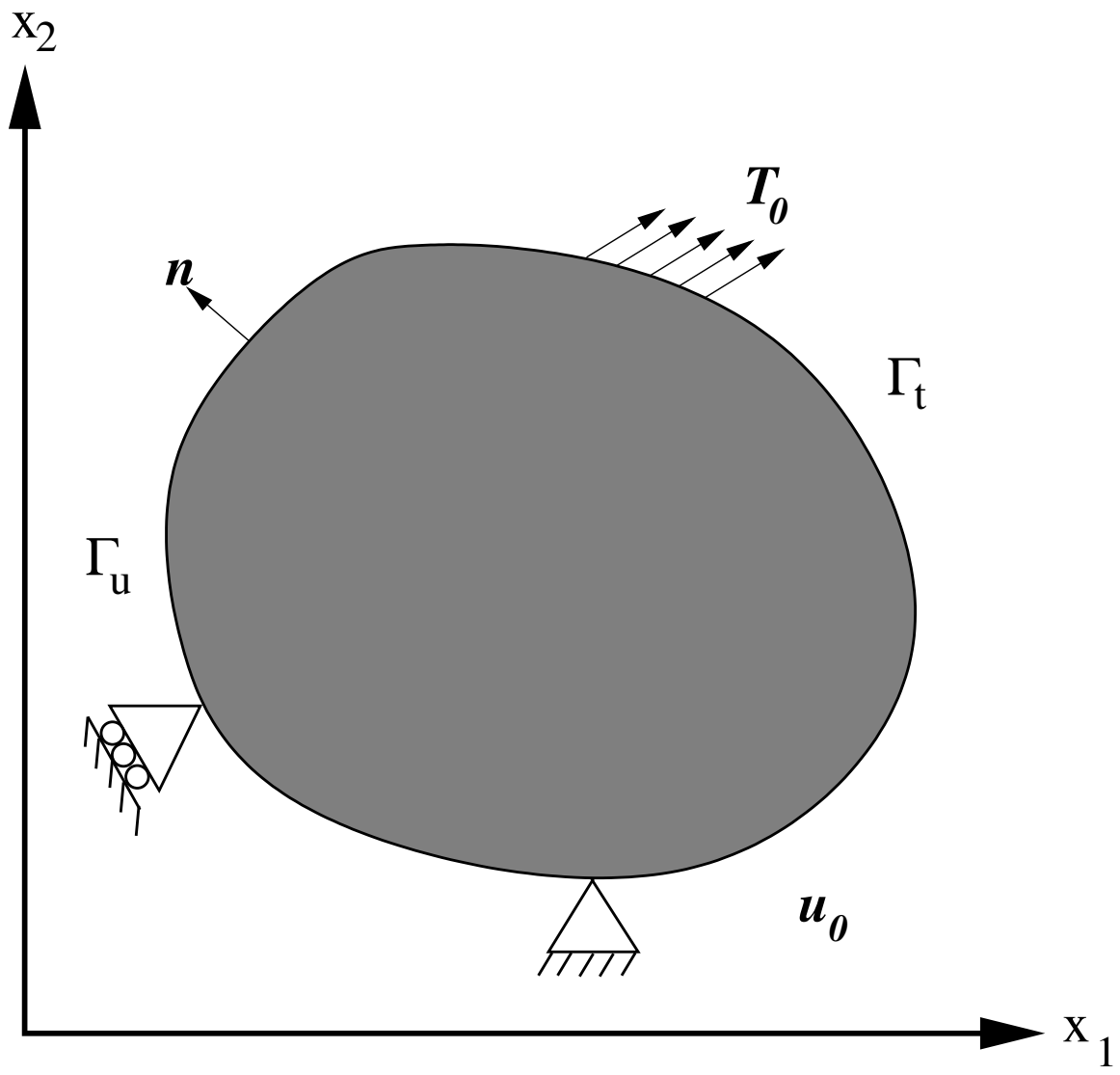

Figure 1: Two-dimensional problem domain.

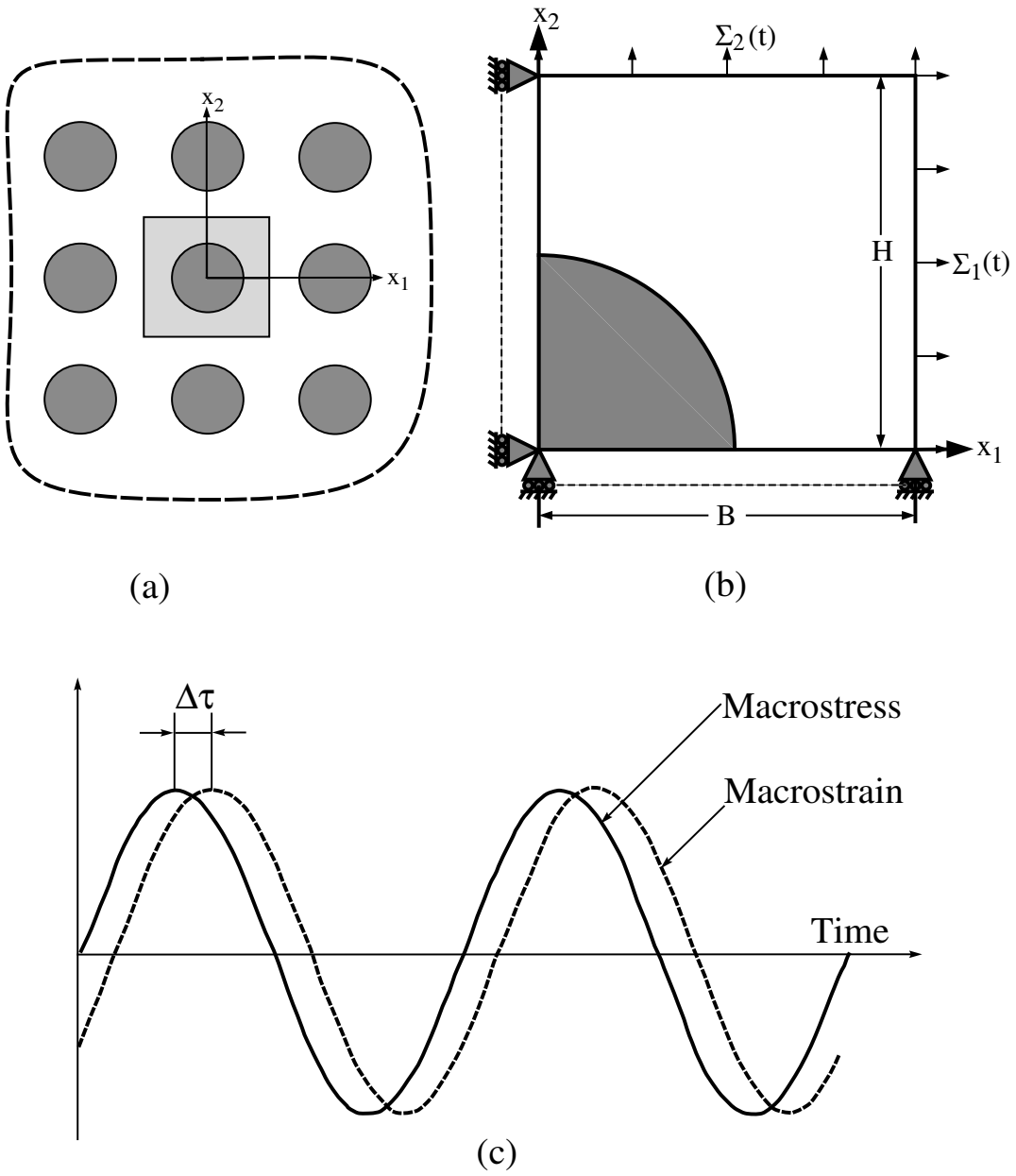

Figure 2: Schematic diagrams showing (a) the square arrangement of cylindrical inclusions and the unitcell. The domain analysed by FEM is shown in (b). The effective $\tan\delta^c$ is calculated from the phase difference between the macrostress and macrostrain responses as shown in (c).

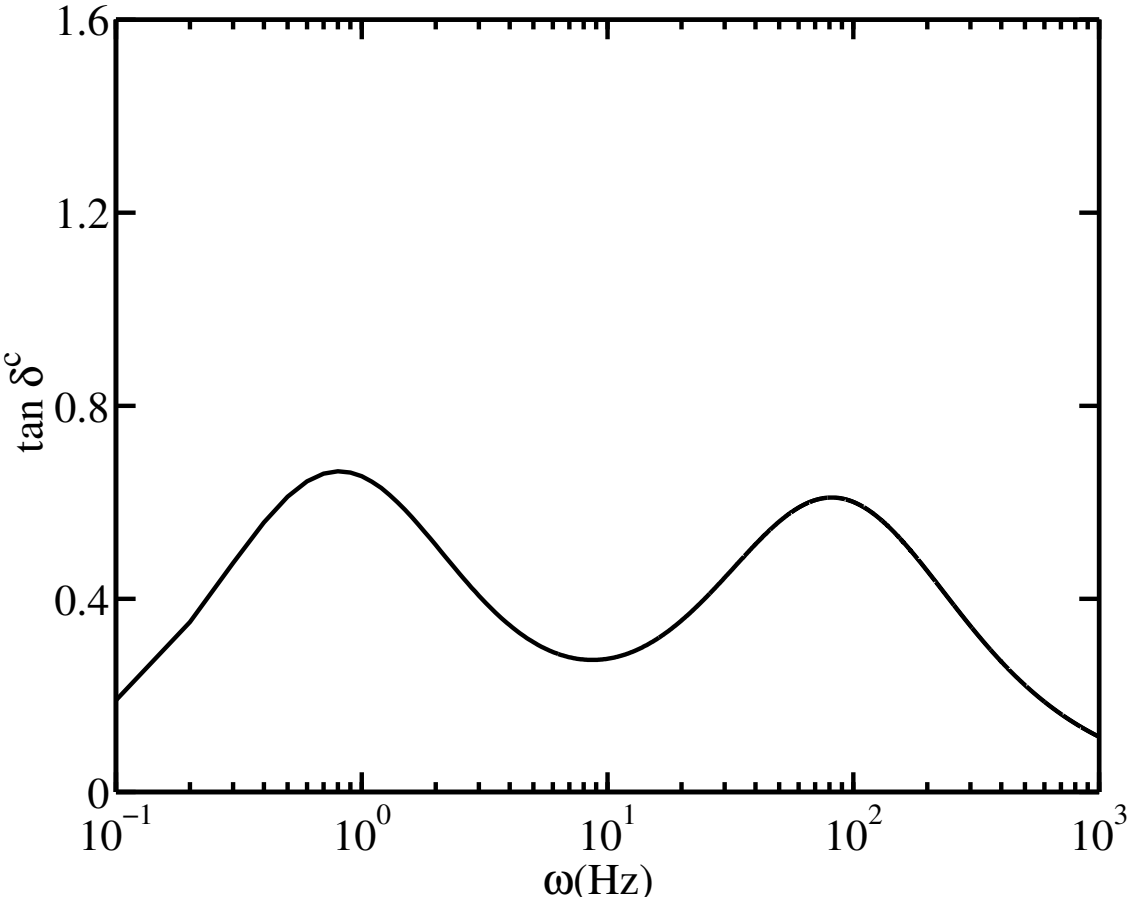

Figure 3: Voigt estimate for two phase viscoelastic composite, with $E^m(t)$=1 + $15e^{-t/0.001}$ MPa and $E^{p_1}(t) = 1 + 10e^{-t/0.1}$ MPa, v^{p_1} =0.3. Peaks occur at $\omega_1 = 0.8$ and $\omega_2 =$ 80 Hz.

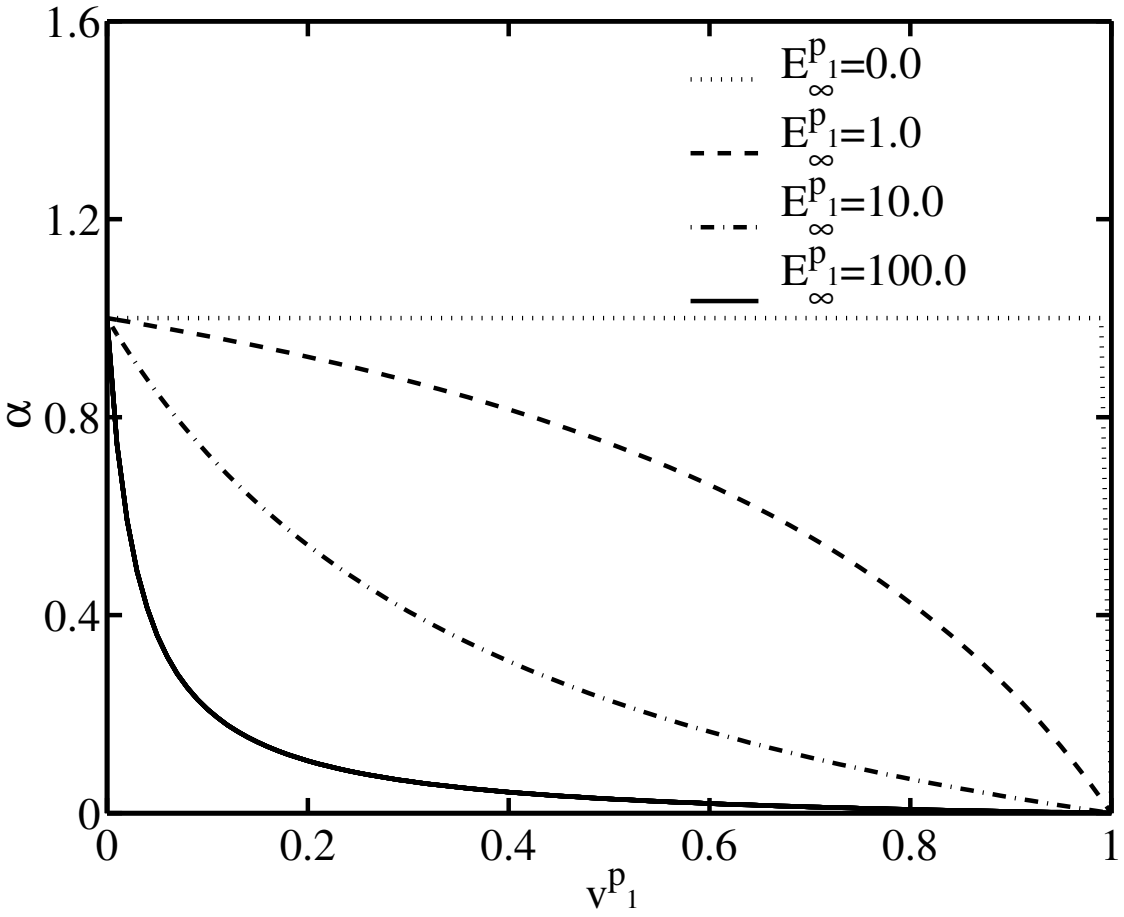

Figure 4: Variation of $\alpha = \max(\tan\delta^c)/\max(\tan\delta^m)$ with volume fraction v^{p_1} of two phase viscoelastic-elastic composites as obtained from simple Voigt estimate.

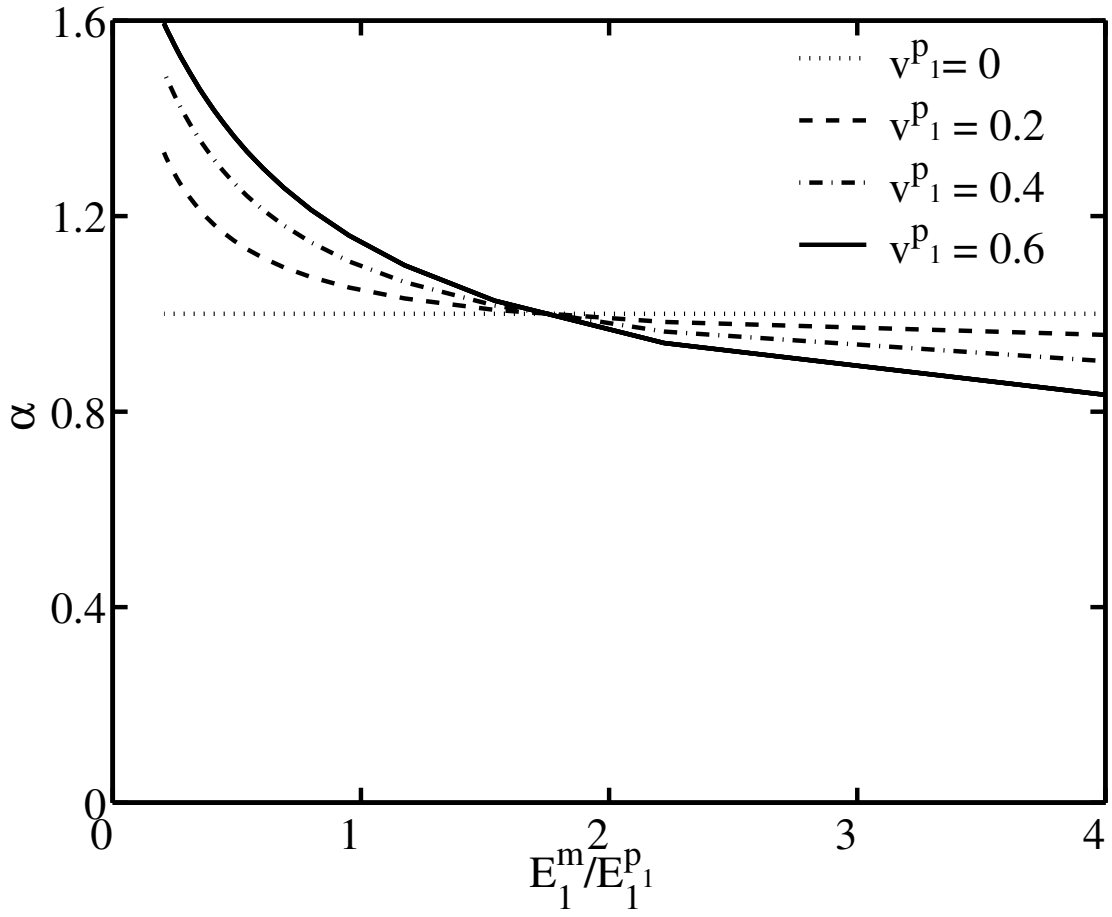

Figure 5: Variation of $\alpha = \max(\tan\delta^c)/\max(\tan\delta^m)$ with $E_1^m/E_1^{p_1}$ for two phase viscoelastic-viscoelastic composites as obtained from simple Voigt estimate.

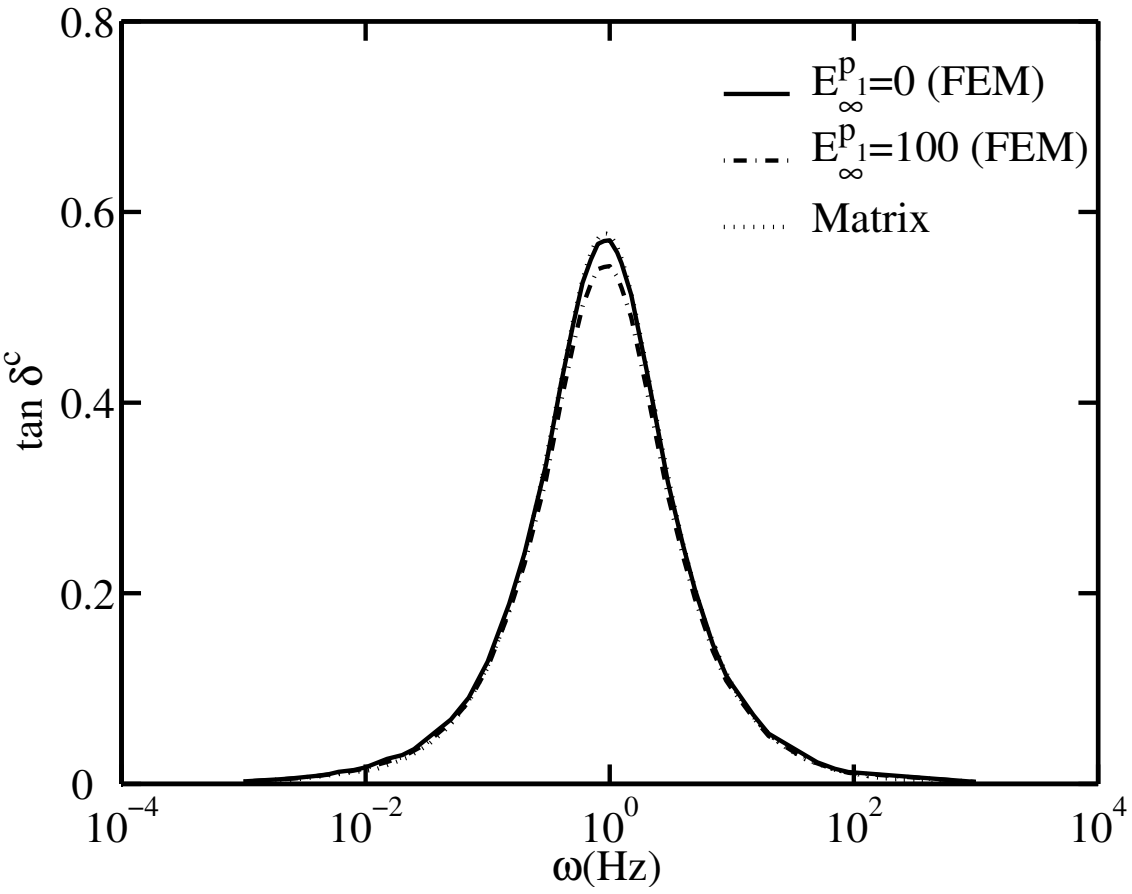

Figure 6: Variation of effective $\tan\delta^c$ with ω for composites with 30% volume fraction of elastic inclusions ($E_\infty^{p_1} = 100$ MPa) and 30% of void ($E_\infty^{p_1} = 0$ MPa).

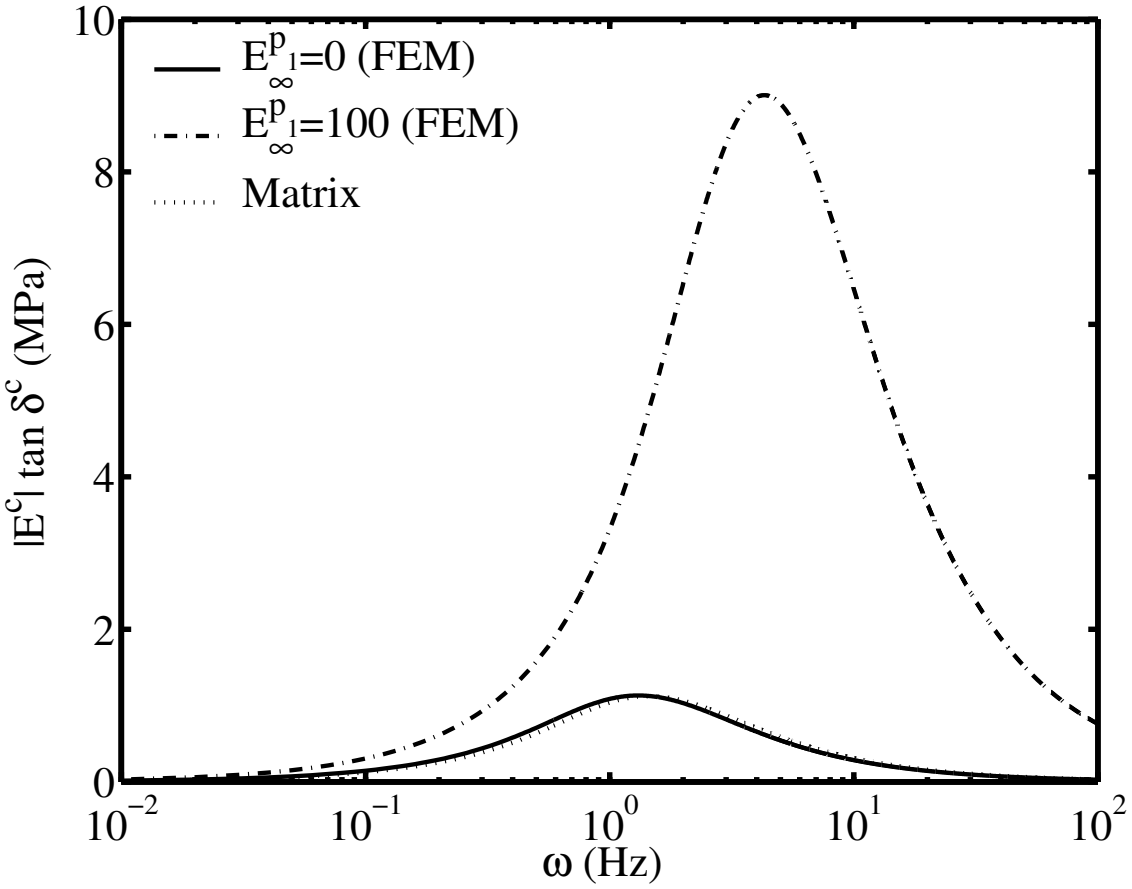

Figure 7: Variation of $|E^c| \tan \delta^c$ with ω of composites with 30% volume fraction of elastic inclusions ($E^{p_1}_\infty = 100$ MPa) and 30% of voids ($E^{p_1}_\infty = 0$ MPa).

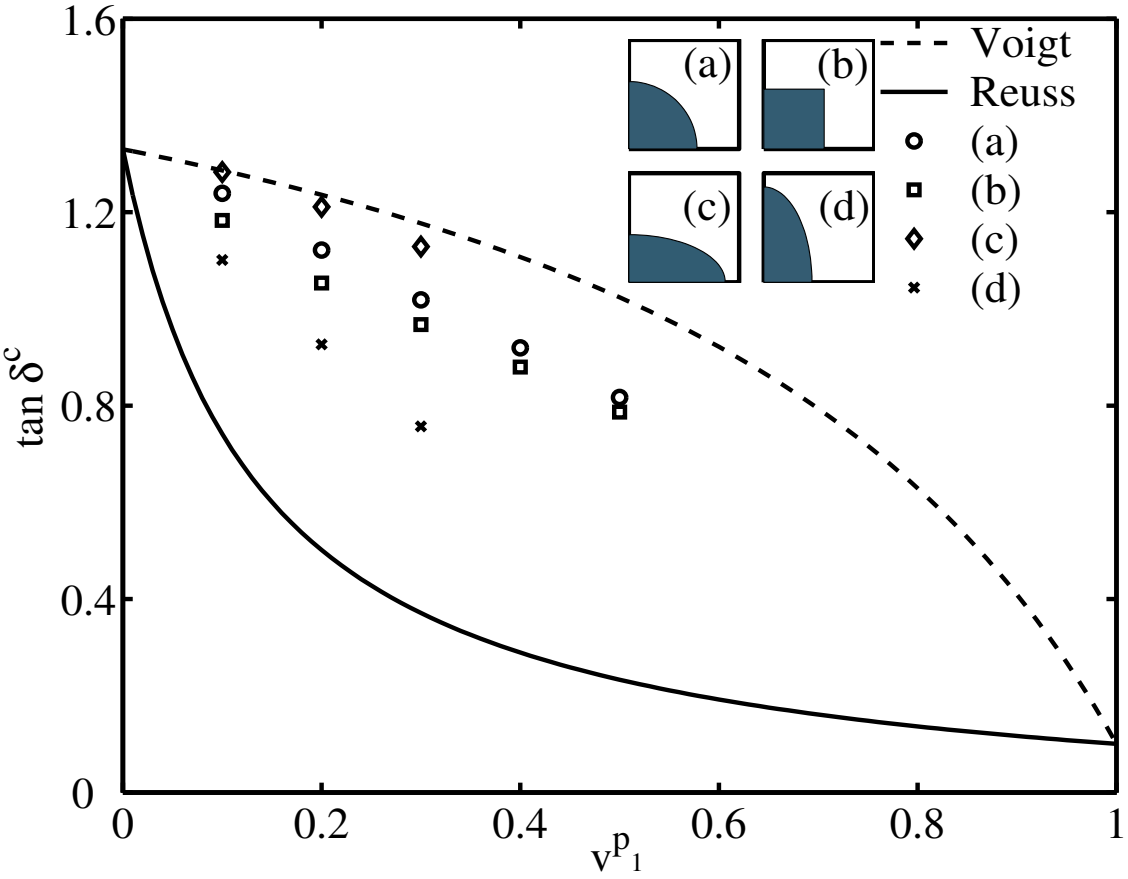

Figure 8: Variation of $\tan \delta^c$ with volume fraction v^{p_1} of inclusions with various cross-sectional shapes. The Voigt and Reuss bounds are also shown.

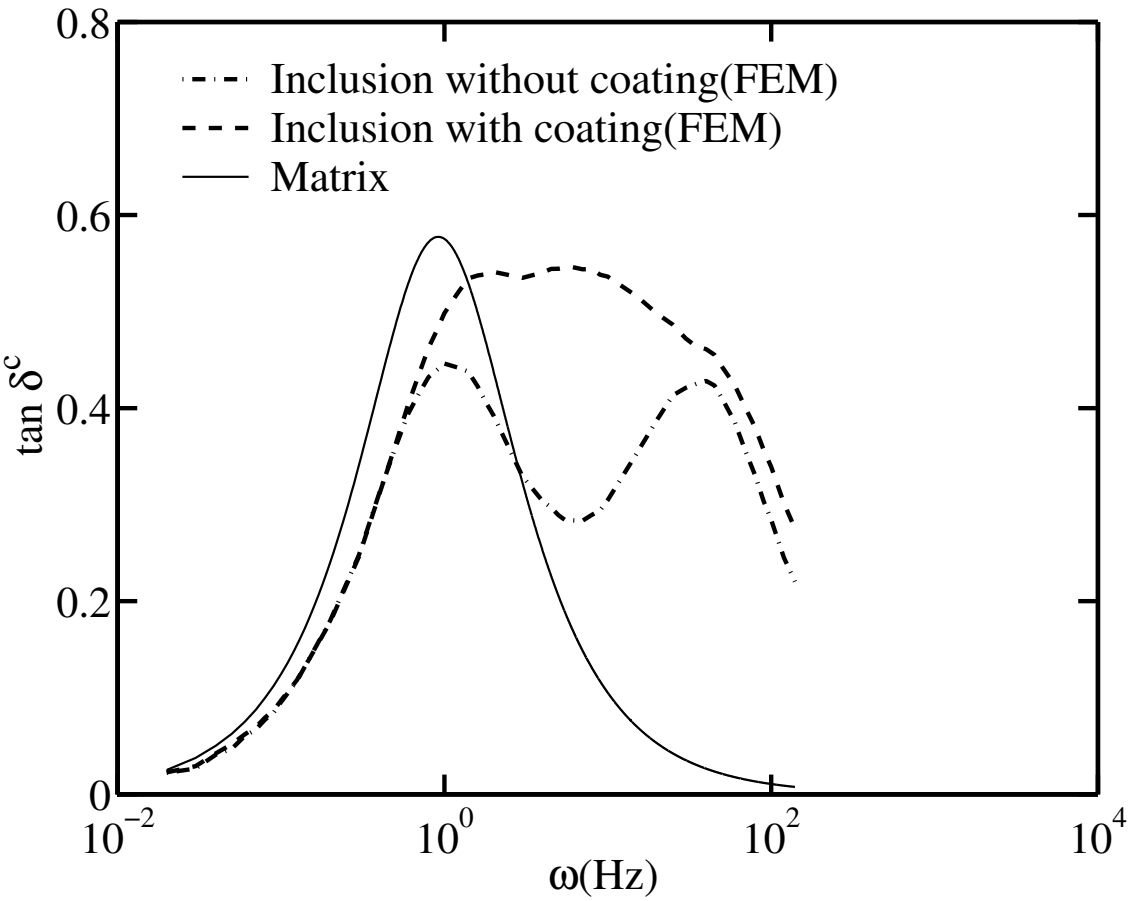

Figure 9: Variation of $\tan\delta^c$ with ω of viscoelastic inclusion with and without viscoelastic coatings. The $\tan\delta^m$ vs. ω response of the matrix is also shown.

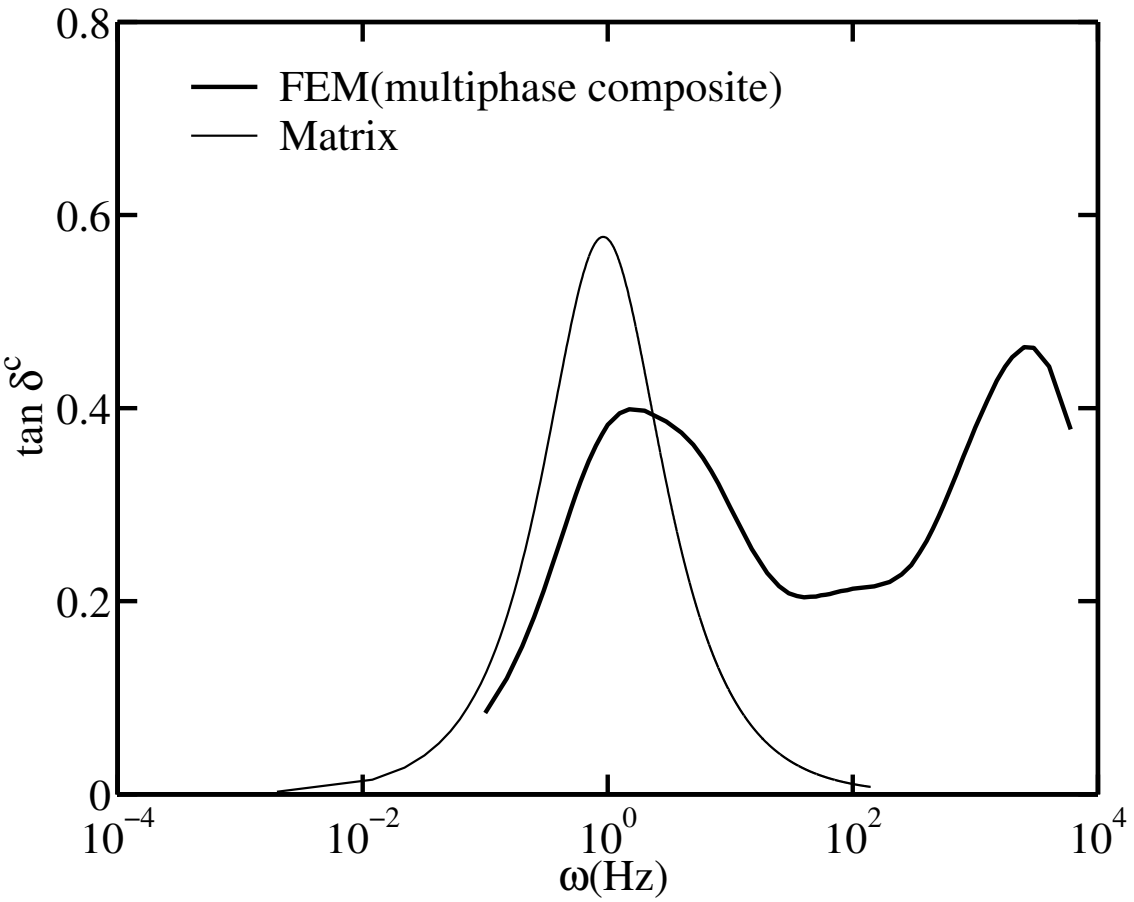

Figure 10: Variation of $\tan\delta^c$ with ω for a viscoelastic composite with layered inclusions. The $\tan\delta^m$ vs. ω response of the matrix is also shown.